Crack Initiation Mechanism in Non-ductile Cracking of Irradiated 304L Stainless Steels under BWR Water Environment

Takeo ONCHI , Kenji DOHI , Marta NAVAS & Wade KARLSEN

ORIGINAL PAPER

Crack Initiation Mechanism in Non-ductile Cracking of Irradiated 304L Stainless Steels under BWR Water Environment

Takeo ONCHI[1,*,†], Kenji DOHI[1], Marta NAVAS[2] and Wade KARLSEN[3]

[1]*Central Research Institute of Electric Power Industry (CRIEPI), 2-11-1, Iwado Kita, Komae-shi, Tokyo 201-8511, Japan*
[2]*CIEMAT, Avda. Compluténse, 22, 28040-Madrid, Spain*
[3]*VTT Industrial Systems, Kemistintie 3A, FI-02044 VTT, Finland*

The deformation behavior and initiation mechanisms of intergranular (IG) and transgranular (TG) cracks in irradiated 304L stainless steel were studied by slow-strain-rate tensile tests in inert gas and simulated BWR water environments, followed by fractographic and microstructural examinations. Neutron irradiation was made in test reactors to fluences of up to $6.2\times10^{20}\,n/\text{cm}^2$ $(E>1\,\text{MeV})$. Intergranular cracking occurred in water above a critical neutron fluence of around $1\times10^{20}\,n/\text{cm}^2$, based on the results of the SSRT tests and SEM fractography. That critical fluence is mechanistically supported by irradiated, deformed microstructures exhibiting dislocation channeling at that fluence, while radiation-induced Cr depletion at the grain boundaries was minor. Transgranular cracking of the irradiated material occurred in water below the critical fluence, initiating in the non-uniformly strained surface region of the test bar in the later stages of plastic deformation. The initiation of TG cracking is hypothesized to be related to a high density of deformation twins. Intergranular cracking is proposed to have initiated where localized slip bands terminated at grain boundaries, while TG cracking is inferred to have initiated at deformation twin boundaries. High stress and strain concentrations at grain/twin boundaries would be the common cause of non-ductile crack initiation.

KEYWORDS: 304L stainless steel, neutron irradiation, intergranular cracking, transgranular cracking, plastic deformation localization, dislocation channeling, deformation twins, grain boundary, twin boundary, stress and strain concentration

I. Introduction

Low carbon stainless steels (SSs)—304L, 316L and 316NG SSs—have been used for vessel internals and piping of BWR in the expectation that they should be more resistant to intergranular stress corrosion cracking (IGSCC) in BWR water environments.[1] This is only because IGSCC has been ascribed to grain boundary Cr depletion produced during cooling down of the welding process. Actually, the promise of such L-grade SSs for SCC resistant materials was supported by extensive pipe tests conducted in the late 70s[2,3] and further verified by slow-strain-rate tensile (SSRT) tests in the late 90s.[4] Nevertheless, there have been an increasing number of SCC incidents of the low carbon SSs in the vessel internals and the pipes in BWR plants.

The 304L SS core shrouds of the US BWR plants exhibited heat affected zone cracking extensively in the 90s. Microstructural examination of the cracked components revealed significant strains adjacent to the weld fusion line,[1] without showing grain boundary Cr carbide precipitations/Cr depletions in the core environment. Characterization of a cracked pipe bend made of 316NG SS also showed very high residual strain close to the fusion line in the welded regions without sensitization.[5] It was found that the strain was attributable to shrinkage strains from the welding process. In both cases, residual strains were a dominant factor for IG cracking without Cr depletion in BWR environment, though cracked portions contain a significant amount of surface cold work, or deformed grains with high dislocation density. Other SCC incidents of the 316L SS core shrouds and primary loop recirculation (PLR) pipes were found in 2002 in the Japanese BWR plants, in which transgranular stress corrosion cracking (TGSCC) initiated in the surface regions heavily cold worked by machining and highly strained by weld deformation, and the cracks then tended to propagate in an IGSCC manner into highly hardened regions.[6] Apparently the occurrences of non-ductile IGSCC and TGSCC cracking on the surfaces of the 304L SS and 316L SS core shrouds and 316NG SS pipes were not due to a corrosion process related to the grain boundary Cr depletion, because the microstructure in low carbon SSs were non-sensitized, but due to mechanically-induced processes in water.

Even if vessel internals made of low carbon SSs have no cold worked layers in the surface region, like the core shroud, they have been subjected to neutron irradiation during service, resulting in radiation induced segregation (RIS) and radiation hardening. Although the amount of the RIS-induced Cr depletion at grain boundaries in low carbon SSs is not enough to cause irradiation assisted stress corrosion cracking (IASCC), the irradiated low carbon SSs are not resistant to IASCC in high temperature oxygenated water in the laboratory tests.[7–9] Therefore, it is still not certain whether or not the RIS induced Cr depletion is really responsible for the occurrence of IASCC.

*Corresponding author, E-mail: takeo.onchi@cao.go.jp
†Present address: *Secretariat of the Nuclear Safety Commission, Cabinet Office, 3-1-1 Kasumigaseki, Chiyoda-ku, Tokyo 100-8970, Japan*
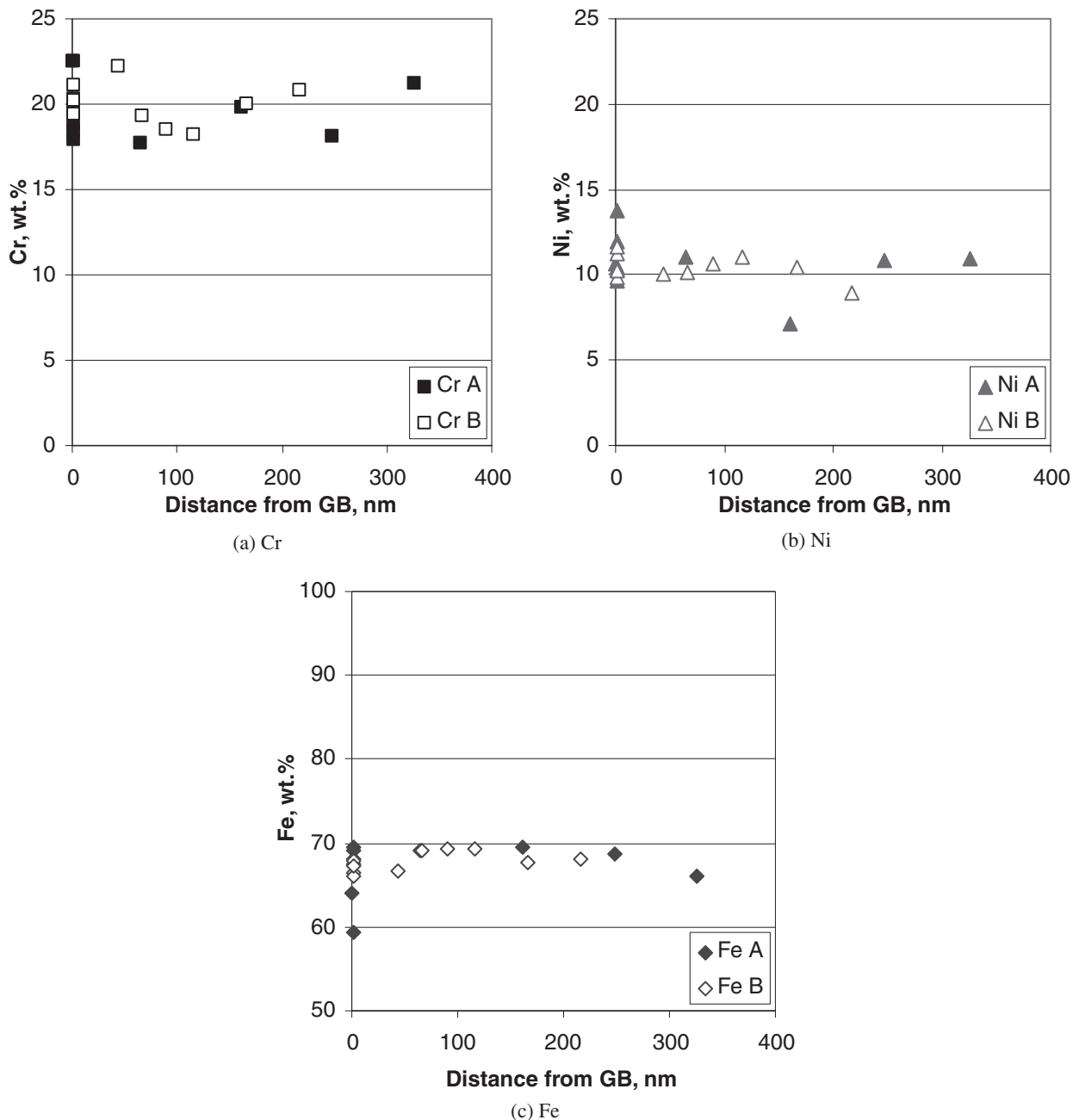
(a) Cr

(b) Ni

(c) Fe

Fig. 1 Concentration profiles of Cr, Ni and Fe at grain boundaries in the unirradiated, thermally treated 304L SS specimen. Analyses were made for two different grain boundaries, A and B.

There is consensus that a threshold fluence for IASCC in high carbon stainless steels is present at around 5×10^{20} n/cm^2 for solution-annealed austenitic SSs in BWR conditions.[10] Concerning the mechanistic process of IASCC, the present authors suggest that IG cracking of the irradiated, sensitized material is principally caused by radiation-induced localization of plastic deformation leading to stress and strain concentrations at the grain boundaries,[11,12] which is simply accelerated by the introduction of an aqueous environment. Occurrences of TGSCC as well as IASCC are still a concern for the degradation of plant component materials, yet the neutron fluence dependent behaviors of IG and TG cracking remain unresolved for the low carbon SSs.

Therefore, the purpose of the present work is to study IG and TG cracking behavior for 304L SSs irradiated to fluences lower than those typically published for IASCC. In the present work emphasis is placed on the mechanical aspects of the crack initiation processes.

II. Experimental

The 304L SS tensile specimens used for this work were fabricated from a plate having a thickness of 13 mm. The specimen has a smooth and flat gauge section 16 mm long, 4 mm wide and 1 mm thick. The chemical composition (in wt%) of the material is: 0.012C, 0.50Si, 1.01Mn, 0.025P,
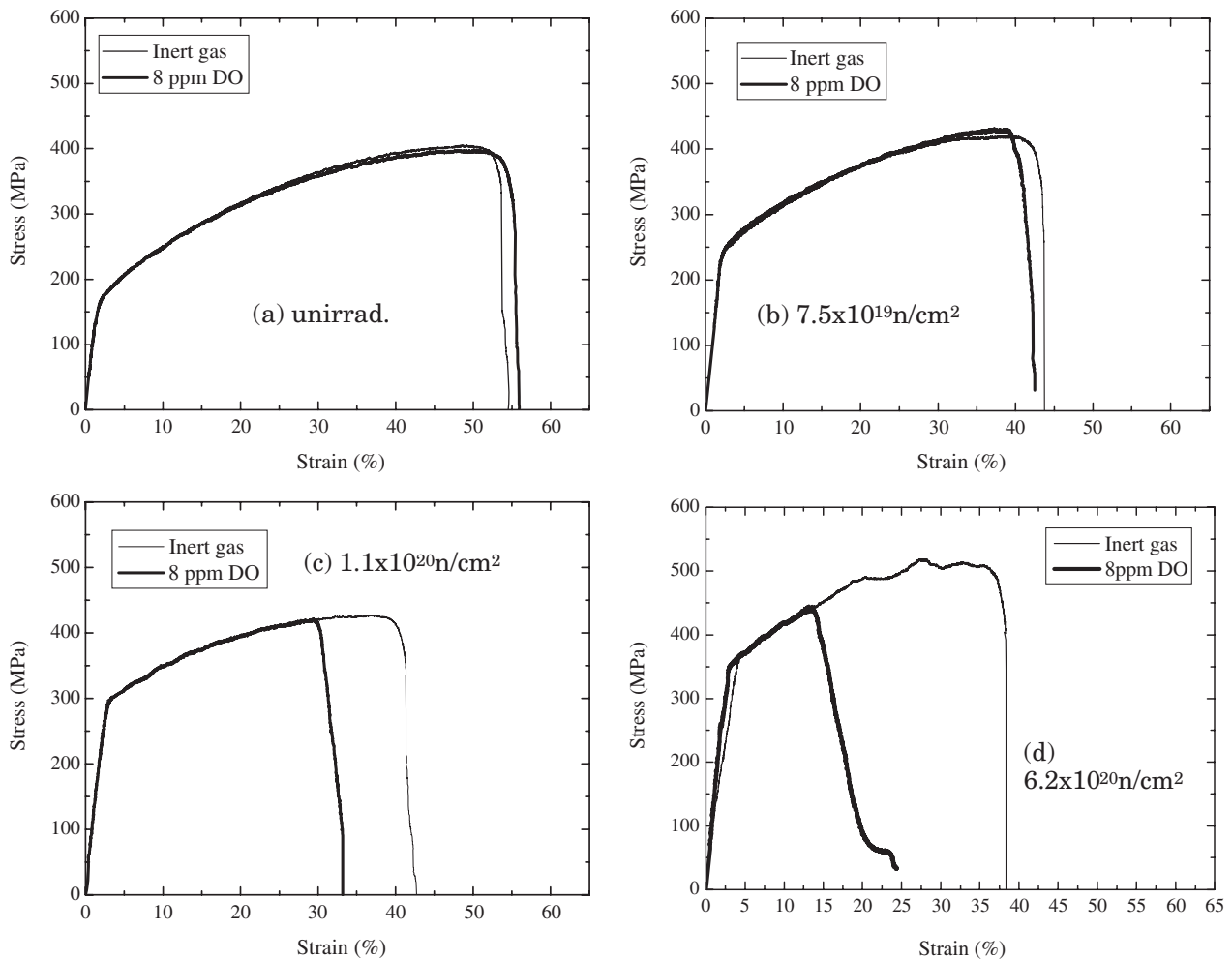
Fig. 2   Stress-strain curves of the 304L SS specimens tested in inert gas and in water

Table 1   Mechanical properties and fracture modes in inert gas, and non-ductile crack initiation strains and IG and TG cracking portions in water

| | Mechanical properties in inert gas | | | | | SSRT tests in water | | | | |
| Fluence (n/cm^2) | Tensile stresses (MPa) | | Elongation (%) | | Fracture mode | DO (ppm) | Non-ductile crack initiation strain | Non-ductile portion | | |
	Yield	Ultimate	Uniform	Non-uniform			(%)	IG	TG	ductile
Unirrad.	168	405	49	5	ductile	8	None	0	0	100
7.5×10^{19}	256	421	40	4	ductile	8	35	0	26	74
1.1×10^{20}	296	427	37	6	ductile	8	25	2	42	56
6.2×10^{20}	368	520	28	10	ductile	8	9	30	31	39

0.018S, 9.93Ni, 18.66Cr, <0.01Co and balance Fe. The specimens were solution annealed, and then thermally treated at 750°C for 100 min followed by 500°C for 24 h. Although the thermal treatment conditions were designed to simulate heat treatments in a welding process, and induced thermal sensitization of high carbon stainless steels,[11] they did not produce any significant gradients in the grain boundary concentration profiles for the principal alloying elements, as shown in **Fig. 1**.

The thermally treated 304L tensile specimens were encap-

sulated with He gas and then neutron irradiated to $7.5 \times 10^{19} \, n/cm^2$ ($E > 1 \, MeV$) at 190°C and to $1.1 \times 10^{20} \, n/cm^2$ at 185°C in Japan Material Test Reactor (JMTR), and to $6.2 \times 10^{20} \, n/cm^2$ at 290°C in Halden Reactor. Neutron fluxes at JMTR and Halden Reactor were 5×10^{13} and $3 \times 10^{13} \, n/cm^2/s$, respectively.

A slow-strain-rate tensile (SSRT) technique was applied for the tests at 290°C in inert gas and in water containing 8 ppm dissolved oxygen (DO), at the CIEMAT hot cell facility. An average strain rate of $3.5 \times 10^{-7} \, s^{-1}$ (a cross head

speed of $0.33\,\mu$m/min) was used. The DO concentrations were maintained during the tests without measurements of corrosion potential. The water conductivity at the inlet and outlet of the test section was less than $0.1\,\mu$S/cm. Mechanical properties of the specimen material were determined from the chart recording during the SSRT tests.

Scanning electron microscopy (SEM) was used to examine detailed fractographic aspects of the fractured specimens tested in inert gas and in water environment. Prior to the SEM, the fractured specimens were ultrasonically cleaned.

Transmission electron microscopy (TEM) observations and grain boundary composition profile analyses of the specimens fractured in inert gas were made at the VTT hot cell facility. TEM foils were extracted from the locations in the grip region, uniformly elongated gauge region, and/ or necked region of the fractured SSRT halves. The pieces were first wet-ground to a thickness of 0.1 mm, and then either 1 or 3 mm diameter disks were punched from them. The 1 mm disks were subsequently embedded in 3 mm diameter disks of non-irradiated SS. The disks were further ground to a thickness of about $80\,\mu$m, and then thinned to electron transparency with a Tenupol Twin-jet electropolisher, using a solution of 30% HNO_3 in methanol at $-30°$C and a voltage of $+7.5\,$V D.C. The perforated slices were examined with a Philips CM200 field emission gun scanning and transmission electron microscope (FEGSTEM) operating at 200 kV. Compositional analyses were carried out utilizing a Noran Voyager energy dispersive X-ray analyzer.

III. Results

1. SSRT Tests

Stress-strain curves of the same fluence materials tested in inert gas and in oxygenated water were superimposed, as shown in **Fig. 2**. It is evident that strain to fracture is lower in water than in inert gas, increasingly so with increasing fluence, particularly above $1.1 \times 10^{20}\,n$/cm^2. The curves for the tests in water also deviated from the ones for the tests in inert gas, suggesting the occurrence of non-ductile fracture in the tests in water. As described later, it was confirmed that non-ductile fracture in the oxygenated water consisted of either IG cracking, TG cracking, or a mixture of those modes. Thus, the strain to the deviation is assumed to be the strain to non-ductile crack initiation from an engineering viewpoint. Although the curve in inert gas at $6.2 \times 10^{20}\,n$/cm^2 is noticeably irregular in the uniform strain region, it is not discernible at present whether or not the anomalous change in the curve is meaningful in the deformation behavior of the irradiated 304L SS. Further work is required to confirm the irregularity.

Table 1 lists the mechanical properties determined from the SSRT test curves for both the inert gas and oxygenated water environments. The tensile properties of the materials tested in inert gas are plotted in **Fig. 3** as a function of neutron fluence. They show that the yield and ultimate tensile strength increase with increasing fluence (Fig. 3(a)), while the uniform elongation decreases and non-uniform elongation increases with fluence (Fig. 3(b)). Although all of those test bars fractured in a ductile manner, the fluence-dependent
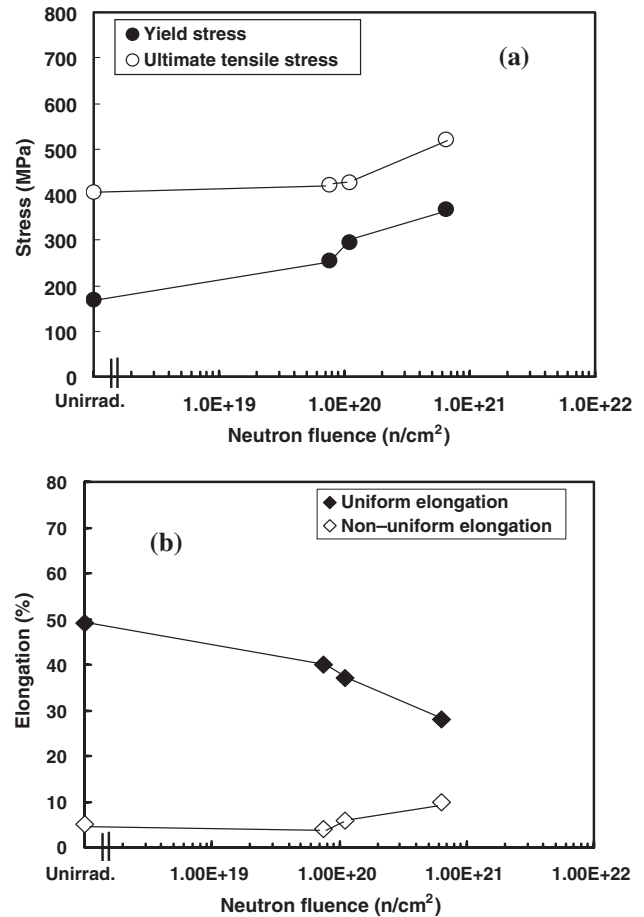

Fig. 3 Tensile properties of the 304L SS specimens as a function of fluence: (a) Yield and ultimate tensile stresses, and (b) Uniform and Non-uniform elongation

changes in ductility were appreciable, especially above about $1 \times 10^{20}\,n$/cm^2.

Figure 4 shows the fracture surfaces of the materials tested in water. It is apparent that the fracture surfaces of all of the irradiated materials show non-ductile fracture modes, consisted of either IG cracking, TG cracking, or a mixture of both (Figs. 4(b), (c) and (d)), while the unirradiated one fractured in a purely ductile manner (Fig. 4(a)). The portions of IG cracking and TG cracking estimated from the results of fractographic examination were included in Table 1.

The portions of IG cracking and TG cracking in the total amount of non-ductile cracking are plotted as a function of neutron fluence in **Fig. 5**. It shows that the total amount of non-ductile fracture (IG+TG) increases with increasing fluence. The portion of IG cracking is very small at around $1 \times 10^{20}\,n$/cm^2, but above this fluence it increases rapidly with fluence, even though no IG cracking was observed in the lower fluence or unirradiated materials (Fig. 5(a)). Thus, the fluence of around $1 \times 10^{20}\,n$/cm^2 would seem to be a critical fluence for fracture in an IG manner. Meanwhile, TG cracking is observed to occur at a fluence as low as $7.5 \times 10^{19}\,n$/cm^2. The amount of TG cracking increases with fluence, reaching a maximum at about 1×10^{20} n/cm^2, beyond which the IG mode becomes increasingly dominant.
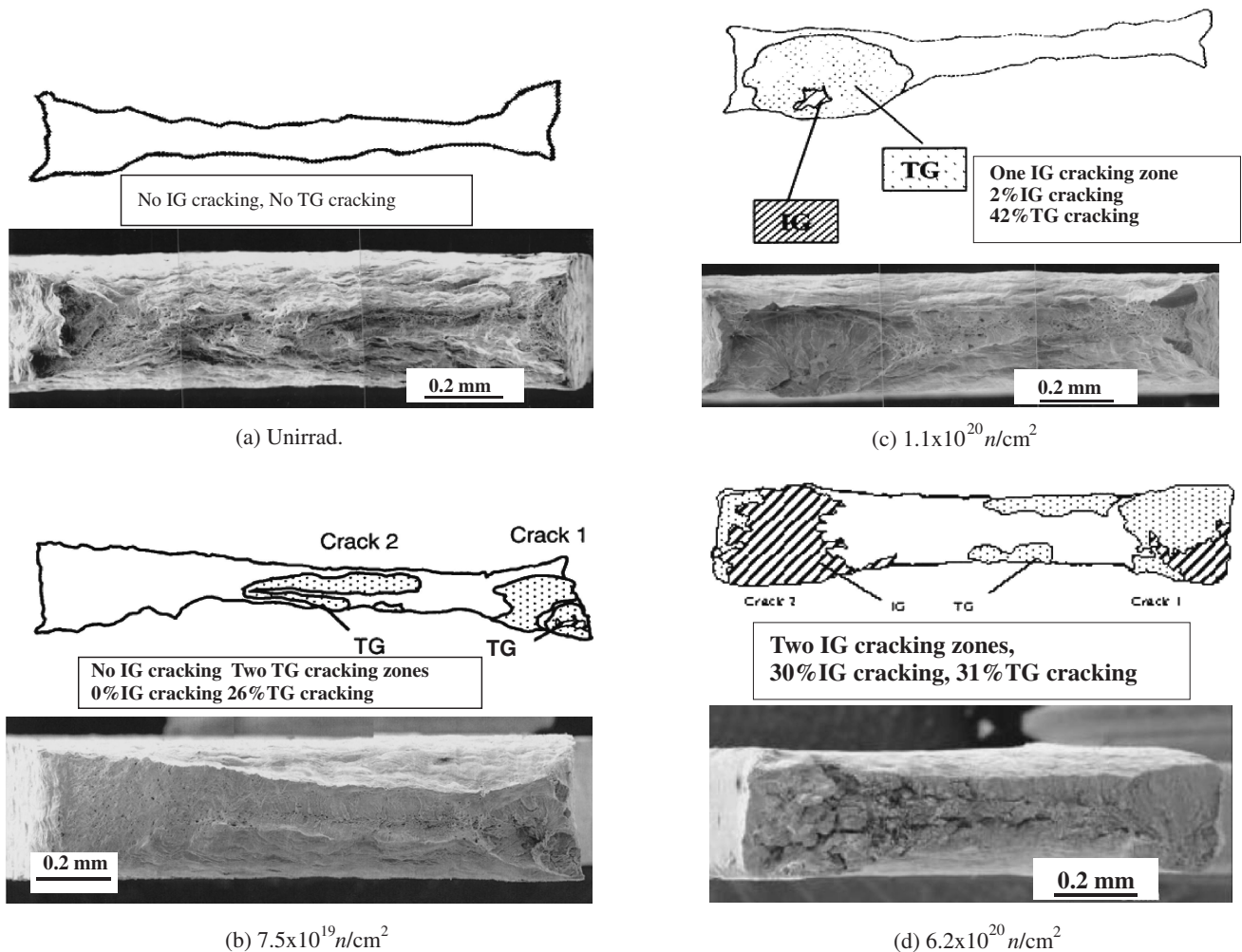
No IG cracking, No TG cracking

0.2 mm

(a) Unirrad.

TG

One IG cracking zone
2%IG cracking
42%TG cracking

IG

0.2 mm

(c) $1.1 \times 10^{20} n/\text{cm}^2$

Crack 2   Crack 1

TG   TG

No IG cracking Two TG cracking zones
0%IG cracking 26%TG cracking

0.2 mm

(b) $7.5 \times 10^{19} n/\text{cm}^2$

Crack 2   IG   TG   Crack 1

Two IG cracking zones,
30%IG cracking, 31%TG cracking

0.2 mm

(d) $6.2 \times 10^{20} n/\text{cm}^2$

Fig. 4 Fracture surfaces of the 304L SS specimens in water

2. SEM Fractographic Examination

More detailed SEM fractographic examinations were carried out to further investigate the mechanisms of non-ductile cracking that occurred in the irradiated materials tested in water.

At $7.5 \times 10^{19} n/\text{cm}^2$ the non-ductile fracture surface was composed solely of 26%TG cracking (see Fig. 4(b)). Details of the appearance of the specimen fractured in water are shown in **Fig. 6**. It can be seen that several possible crack initiation sites are present on the surface region close to fracture face, marked with white circles in Fig. 6(a), and that the fracture surface correspondingly shows a TG cracking mode (Fig. 6(b)). Such features in the surface regions, shown more closely in Figs. 6(c) and (d), were most likely produced by plastic strain localization, which could promote the TG crack initiation.

Figure 7 presents the fracture surface of the specimen exhibiting 2%IG and 42%TG cracking at $1.1 \times 10^{20} n/\text{cm}^2$ (see Fig. 4(c)). Only a small region of IG fracture surrounded by TG cracking was identified. The IG fracture, corresponding to approximately only one grain, does not exhibit a clear IG crack shape on the whole, but that is probably because the mechanism of IG cracking is not yet very dominant at the critical fluence.

Figure 8 shows details of the fracture behavior of the $6.2 \times 10^{20} n/\text{cm}^2$ material tested in water, which showed 30%IG and 31%TG cracking (See Fig. 4(d)). Fracture occurred at two different sites transversely to the specimen gauge section (Fig. 8(a)). IG crack facets are mostly decorated with deformation step markings (Figs. 8(b) and (c)), though covered with thick corrosion product depositions. Localized deformation band traces (Fig. 8(d)) and small secondary cracks (Fig. 8(e)) are revealed on the specimen surface close to the fracture face, suggesting that IG cracks initiated at the intersection of localized deformation bands, linked to each other and grew until final ductile failure (Fig. 8(f)).

3. TEM Microstructural and Microchemical Examination

Grain boundary chemistry analyses and characterization of the undeformed and deformed microstructures were made by FEG-STEM examination of the different materials deformed to fracture in inert gas environment.

Typical unirradiated, deformed microstructures are shown in **Fig. 9**. The bulk of the microstructure in the uniformly strained region is composed of two principal features–a cellularized structure of a high density of dislocations structure, and a sparse distribution of long bands having a slightly dif-
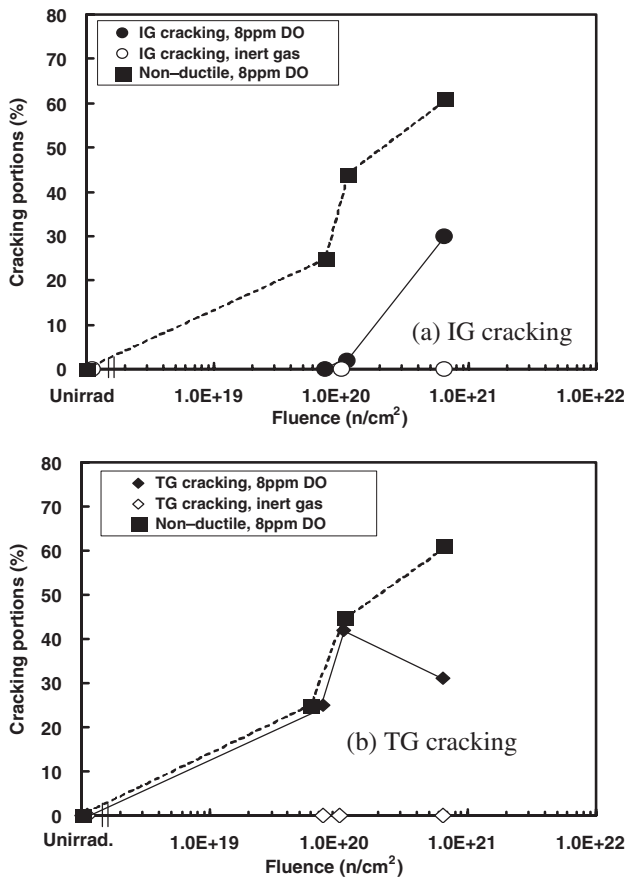
Fig. 5 The non-ductile portions as a function of neutron fluence in water: (a) IG and Non-ductile cracking and (b) TG and Non-ductile cracking

ferent crystal orientation from that of the surrounding material (Fig. 9(a)). Selected-area diffraction (SAD) analysis showed the bands to be hexagonal close-packed (hcp) epsilon martensite, brought about by the accumulation of stacking-faults on every other close-packed plane in the austenite, indicative of planar slip. In the non-uniformly deformed region closer to the fracture face the microstructures were basically similar to those in the uniformly strained region, except that some particular, isolated regions also contained some shorter, small bands shown by SAD analysis to be hexagonal close-packed (hcp) epsilon martensite (marked with white circle in Fig. 9(b)) and face centered-cubic deformation twins (marked with black circle in Fig. 9(b)). On the whole though, the deformation in the unirradiated material occurred overwhelmingly by classic uniform dislocation movement.

At 7.5×10^{19} n/cm^2, where 26%TG cracking but no IG cracking were observed in the tests carried out in water (Fig. 4(b)), radiation damage defects were invisible yet. **Figure 10** shows microstructures in the non-uniformly deformed region close to fracture face, predominantly consisting of a high density of dislocations segregating to some particular bands (Fig. 10(a)), with a broader, twin-looking band that was populated by many, very distinct microtwins (Fig. 10(b)). Close inspection of regions of high dislocation

density also revealed a dense population of nano-/micro-twins. Bands of epsilon martensite were also occasionally observed, symptomatic of the planar slip.

At 1.1×10^{20} n/cm^2, a small percent of IG fracture and large percent of TG cracking occurred in the tests conducted in water (Fig. 4(c)). As shown in **Fig. 11**, the mildly-deformed material from the grip portion of the test-bar fractured in inert gas exhibited clear dislocation channel structures among the radiation-induced "black-spots." Dislocation tangles are also evident at the intersections of the channels. Visible lower in the image are steps which have been induced in some channels upon being intersected by another channel (Fig. 11(a)). Closer inspection of the channels shows the presence of some larger irradiation defects still remaining within the bands (Fig. 11(b)).

Figure 12 shows the highly deformed microstructure close to fracture face of that 1.1×10^{20} n/cm^2 specimen. The dislocation-dominant microstuctures show signs of segregation of dislocations to particular bands (Fig. 12(a)). On the other hand, some micro-/nanotwins are also evident, in addition to many irradiation-induced "black-spots" still remaining (Fig. 12(b)). The twinning most likely occurred due to the higher critical resolved shear stress (CRSS) achieved at that location, in part due to the greater strain accumulation present near the fracture face and in part due to the irradiation-induced defect population remaining in the material.

At 6.2×10^{20} n/cm^2, a large amount of IG cracking together with TG cracking occurred in water (Fig. 4(d)). Typical deformed microstructures in the uniformly strained region of the sample tested in inert gas are shown in **Fig. 13**. The microstructures were primarily dislocation-dominant, showing clear signs of segregation of dislocations to particular bands within grains (Fig. 13(a)). Waviness in the contrasts, corresponding to local alterations in the crystal lattice orientation, was visible in the regions adjacent to the grain boundaries (Fig. 13(b)). That waviness suggests strain concentrations in the grain boundary areas, brought about by the inhomogeneous planarized slip deformation.

Segregations of major alloy elements at the grain boundaries, particularly the Cr concentration gradient, were examined by FEG-STEM analyses on the samples irradiated to different fluences. **Figure 14** shows Cr, Ni and P concentration profiles at different fluences. It is seen that the concentration gradients of these chemical elements across the grain boundary are unchanged at the unirradiated condition and 7.5×10^{19} and 1.1×10^{20} n/cm^2, whereas they are significantly different at 6.2×10^{20} n/cm^2, namely, Cr depletion and Ni enrichment occurred with a narrow peak of P segregation. Although a slight RIS-induced Cr depletion was detected, a high level of Cr concentration was still maintained at the grain boundaries. However, direct comparisons of absolute Cr concentrations between different fluences are difficult with a great degree of confidence, since the exact electropolishing procedure employed for each foil can result in a different chrome oxide layer thickness, and therefore affect the absolute level of Cr measured. That does not, however, affect the particular profile measured at the grain boundary.
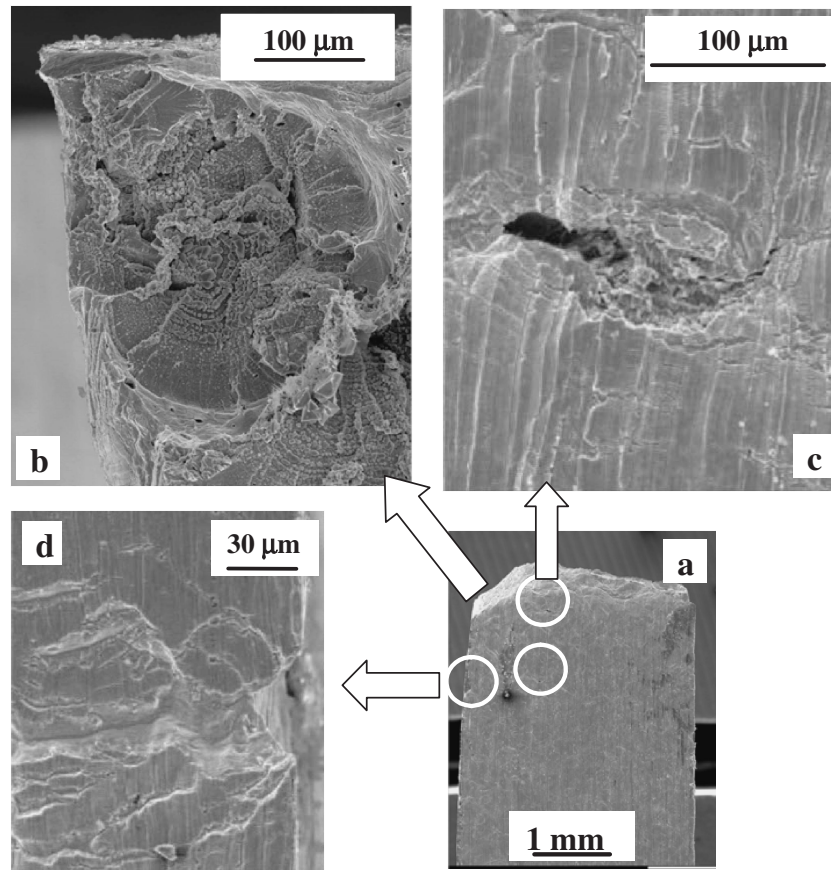
Fig. 6 Fractographic appearances of the 7.5×10^{19} n/cm^2 specimen in water; (a) general surface view, (b) TG crack surface, and (c) and (d) TG crack initiation sites

IV. Discussion

1. Non-ductile Cracking Behaviors in Water

The results of SSRT tests in water and fracture surface observations showed that a very small IG fracture occurred at around 1×10^{20} n/cm^2, and above that fluence the amount of IG cracking increased with increasing fluence (Fig. 5(a) and Fig. 7). This indicates that a critical neutron fluence above which IG cracking occurs in water is present at around 1×10^{20} n/cm^2. TG cracking occurred at a lower fluence, as low as 7.5×10^{19} n/cm^2. The amount of TG cracking reached a maximum at the critical fluence, and then tended to reduce at a higher fluence as the contribution of IG cracking became more dominant (Fig. 5(b)).

The results of TEM examination on material tested in inert gas revealed that below the critical fluence radiation damage defects were invisible yet, and deformed microstructures were primarily of cellularlized dislocations with some tendency towards planarized slip. At around the critical fluence, however, dislocation channeling structures were evident along with clearly visible radiation damage defects in mildly-deformed region (Fig. 11(a)) and in more highly deformed regions the dislocations were more strongly segregated to particular bands (Fig. 12(a)). Thus the critical fluence would appear to mark a transition towards more inhomogeneous plastic deformation, by dislocation slip preferentially occurring along prior channels. Meanwhile, the re-

sults of FEGSTEM analyses indicated that Cr and Ni concentration gradients at grain boundaries remained essentially the same from the unirradiated condition up to lower fluences of 1.1×10^{20} n/cm^2, whereas Cr depletion and Ni enrichment occurred at 6.2×10^{20} n/cm^2 (Figs. 1 and 14). Therefore the critical fluence of around 1×10^{20} n/cm^2 for IG cracking in the irradiated 304L SS is supported in both an engineering capacity by the SSRT tests in water and the SEM fractography, and mechanistically by the TEM micrography of specimens tested in inert gas.

The critical fluence of around 1×10^{20} n/cm^2 for IG cracking of the irradiated 304L SS is the same as that for the irradiated, thermally-sensitized 304 SS[11] that were irradiated in the same capsules and tested in the same test loop with the SSRT machine. It should be noted that the threshold fluence of about 5×10^{20} n/cm^2 for IASCC in the BWR-irradiated austenitic SSs[10] is a consensus from an engineering viewpoint. The threshold fluence for the solution-annealed 304 SS material is based on the results of the SSRT tests in water and the SEM examination, in contrast to the critical fluence for onset of channel deformation observed for the 304L SS in the present work. In other words, although the threshold fluence for the 304 SS has not been confirmed mechanistically by examination of the irradiated, deformed microstructure or microchemistry profiles at grain boundaries, it is nevertheless likely that the critical fluence for IG cracking in the irradiated 304L SS is consistent with the mechanism un-
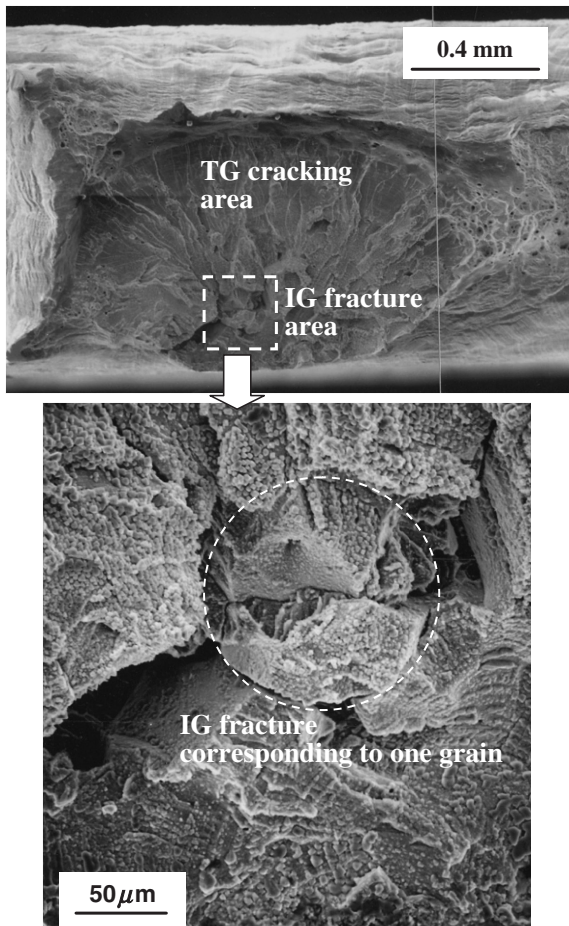
Fig. 7 Fractographic appearances of the $1.1 \times 10^{20}\, n/\mathrm{cm}^2$ specimen in water, consisting of a small amount of IG fracture area surrounded by TG cracking

Fig. 8 Fractographic appearances of the $6.2 \times 10^{20}\, n/\mathrm{cm}^2$ specimen in water; (a) general surface view, (b) and (c) IG crack facets, and (d), (e) and (f) specimen surface cracks

derlying the threshold fluence for IASCC in other irradiated austenitic SSs.

2. Mechanism of IG Crack Initiation

The superimposed stress-strain curves in inert gas and in water above the critical fluence suggest that IG cracking initiates in the early stage of slip deformation during straining to maximum stress (Figs. 2(c) and (d)). **Figure 15** depicts engineering strain to non-ductile crack initiation in water as a function of neutron fluence, compared with uniform elongation. Although engineering strain to non-ductile crack initiation and uniform elongation decrease with increasing fluence, the difference between them becomes larger, in particular above the critical fluence. This indicates that the initiation of IG cracking comes earlier with increasing fluence.

To examine processes of IG crack initiation in the uniform strain region, interrupted SSRT tests were carried out. A $6.4 \times 10^{20}\, n/\mathrm{cm}^2$ specimen was strained to about 4% (a total strain of 7%) in water and unloaded, followed by detailed specimen surface observations. Several small incipient cracks were revealed on both sides of the specimen gauge section. The specimen was then loaded and strained to about 9% (a total strain of 13%) in water. More cracks were present on both sides of the specimen, as shown in **Fig. 16**. The
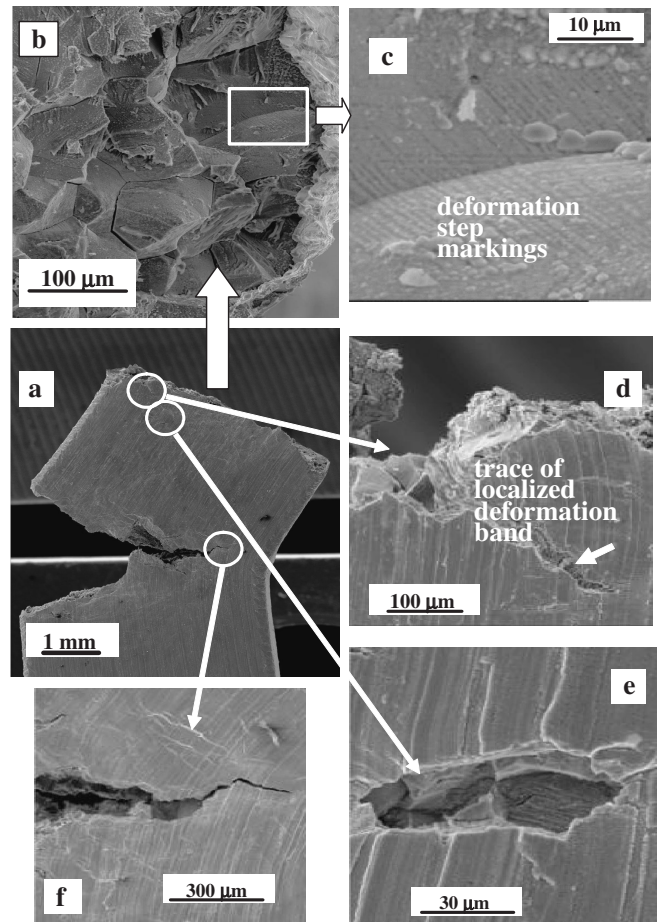
cracks were distributed from one end to the other over the entire specimen gauge length (Fig. 16(a)). All the cracks grew transversely to the tensile direction (Figs. 16(b), (c) and (d)). A large crack extended from one edge to the middle of the gauge width near the grip (Fig. 16(e)), exhibiting IG crack facets (Fig. 16(f)). It is noted that not only did the cracks identified at 4% strain grow during the test to 9% strain, but that a few new, additional cracks were also detected at 9% strain. This indicates that both the number of IG crack initiation sites in the uniform strain region and the size of the IG cracks increased with increasing strain.

The classical mechanism of IG crack initiation in oxygenated water for the irradiated austenitic SSs has been explained in terms of the RIS-induced Cr depletion at grain boundaries in the same way as that for the thermally sensitized 304 SS. Nowadays, however, the role of the Cr depletion on IASCC initiation is disputable. For instance, Busby *et al.*[13] insist that the Cr depletion is not the primary determinator for IASCC susceptibility in oxygenated water, whereas Fukuya *et al.*[14] indicate that the grain boundary segregation, probably Cr depletion, was sufficient to cause IASCC in oxygenated water. In the present work there was no appreciable Cr depletion at grain boundaries of the 304L SS in the unirradiated condition or at fluences of up
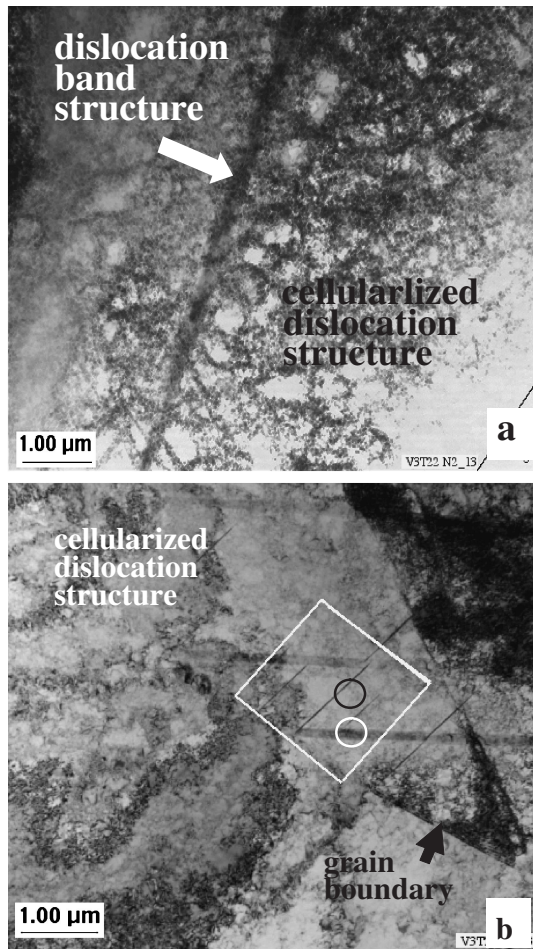
Fig. 9 Typical unirradiated, deformed microstructures; (a) cellularized dislocation structure in a uniformely-deformed region, and (b) two kinds of long, narrow deformation induced bands (in the rectangle) in-non-uniformly deformed region.

Fig. 10 Typical deformed microstructures of the $7.5\times10^{19}\,n/cm^2$ material; (a) segregated dislocation band structure and (b) deformation twins

to around the critical fluence, while only a small amount of Cr depletion was detected at $6.2\times10^{20}\,n/cm^2$. Nevertheless, IG cracking occurred above around $1\times10^{20}\,n/cm^2$, indicating that the RIS-induced Cr depletion is not responsible for the IG crack initiation in oxygenated water. Therefore, it is evident that Cr depletion at the grain boundary was not a primary factor for crack initiation in oxygenated water.

Radiation induced, inhomogeneous plastic deformation would be an alternative to Cr depletion for IG crack initiation in water. Uniform elongation of the 304L SS is significantly smaller at $6.2\times10^{20}\,n/cm^2$ than at the lower fluences (Fig. 3(b)). The reduction in uniform elongation due to neutron irradiation is ascribable to dislocation channeling structures,[15] in general. Thus we have to pay attention to the phenomenon of dislocation channeling in the irradiated material. Apparently, the occurrence of inhomogeneous slip deformation typified by dislocation channeling is a key step to initiate IG cracking of the irradiated 304L SS in water, because the critical fluence for IG cracking is equivalent to that for dislocation channeling in the irradiated 304L SS, as discussed above.
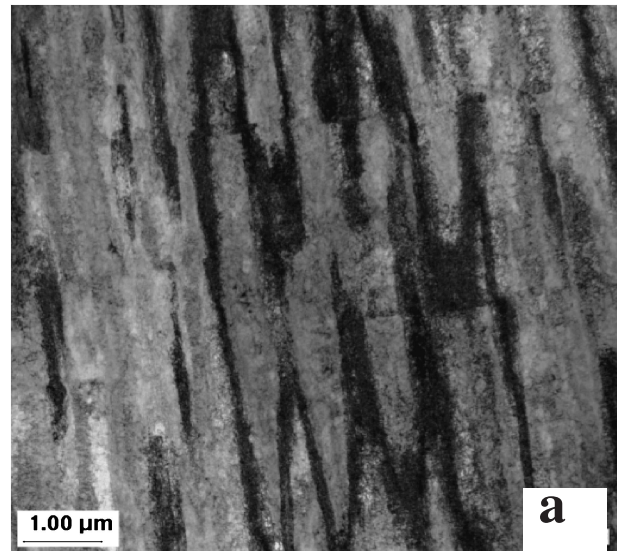
Dislocation channeling structures in irradiated 304L SSs

have been observed by several workers. For examples, Victoria et al.[16] showed TEM images of dislocation channels in 304L SS neutron-irradiated to 1.5 dpa and deformed at 550 K. Cole et al.[17] reported to have observed both dislocation channeling and deformation twinning in 304L SS heavy ion-irradiated up to 5 dpa and deformed at 288°C. Carter et al.[18] also found dislocation channels in 304L SS proton-irradiated to 1 dpa and deformed at 288°C. In the present work, it is around $1\times10^{20}\,n/cm^2$ (~0.16 dpa) that dislocation channeling structures were identified in the irradiated 304L SS. This fluence level is the lowest among those reported in the literatures and corresponds to the critical fluence for IG fracture in water.

A more careful investigation of the dislocation channel structures was made to gain mechanistic insights into the IG crack initiation process in the irradiated 304L SS. The geometrical pattern of dislocation channel structure shows steps that have been induced in some channels upon being
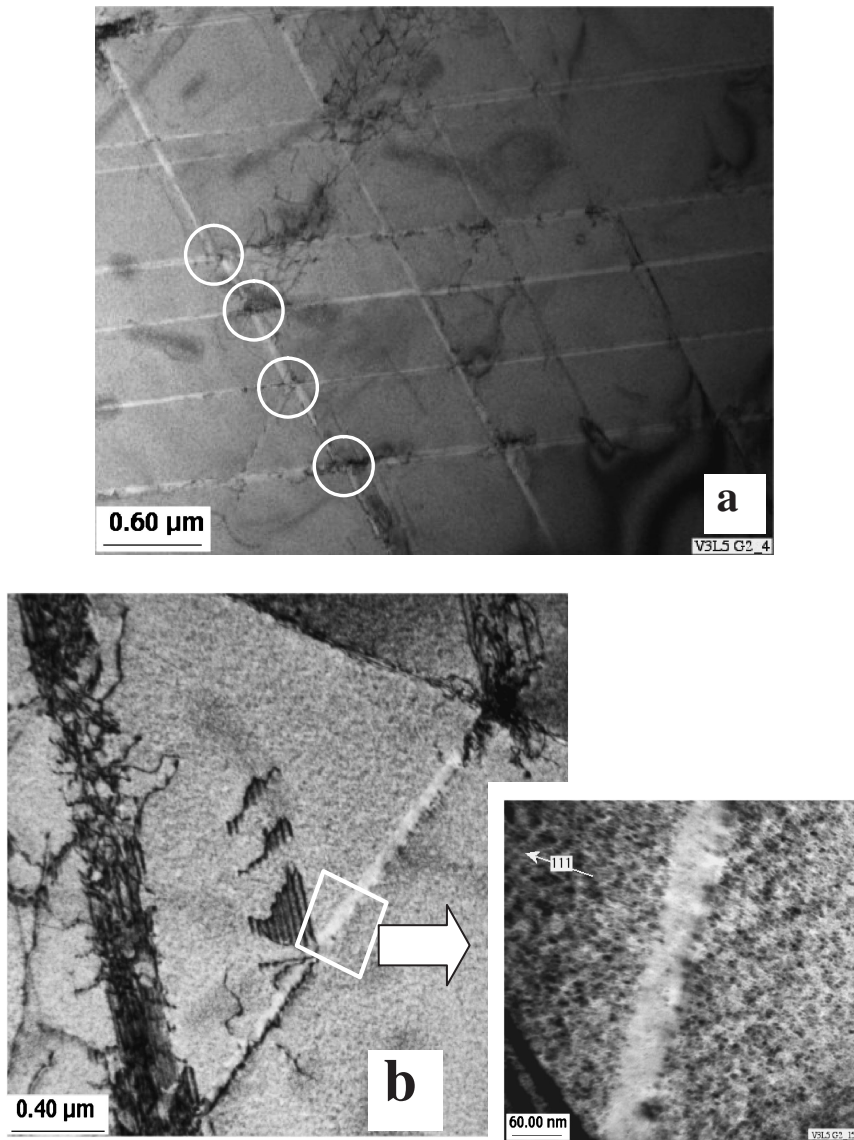
Fig. 11 Clear dislocation channeling structure of the mildly-deformed region of the $1.1 \times 10^{20} \, n/cm^2$ material; (a) low magnification image, and (b) high magnification image

intersected by another channel (circled in Fig. 11(a)). In IG facets of the fracture surface of the $6.2 \times 10^{20} \, n/cm^2$ material, deformation step markings are identified, though covered with corrosion products deposition, as was shown in Figs. 8(b) and (c). Such deformation step markings were more clearly observed in the IG facets of fracture surface in inert gas and in water for the irradiated, thermally-sensitized 304 SSs irradiated to higher fluences.[11,12] The step markings in dislocation channeling structures as identified in irradiated, deformed microstructures correspond to those fractographically observed in the irradiated austenitic stainless steels. Thus, such slip deformation step markings in the irradiated, deformed microstructures and fractographic IG facets are important mechanistic evidence supporting a mechanically-induced process of IG crack initiation in the irradiated material.

Figure 17 represents a high magnification image of the intersecting points of dislocation channels, showing a very

significant dislocations pile-up. It is suggested from this image that such high dislocation densities at the intersecting point of the channels would promote local stress and strain concentration at the intersecting points. Further, when such dislocation channels and/or localized deformation bands impinged against grain boundaries, it can be reasoned by analogy that a sufficiently high level of stress concentrations would be generated at the grain boundaries of the irradiated material. The initiation of IG cracks in water would occur so as to relieve stress and strain concentrations at grain boundaries. In the interrupted SSRT tests, as presented earlier, small IG cracks initiated at the grain boundaries at about 4% strain and then grew to larger cracks after straining to about 9%, with new cracks also initiated during the straining. This indicates that the earlier onsets of localized plastic deformation and subsequent interaction with grain boundaries in local regions would lead to the earlier initiation of IG cracks and their wider distribution over the entire gauge section
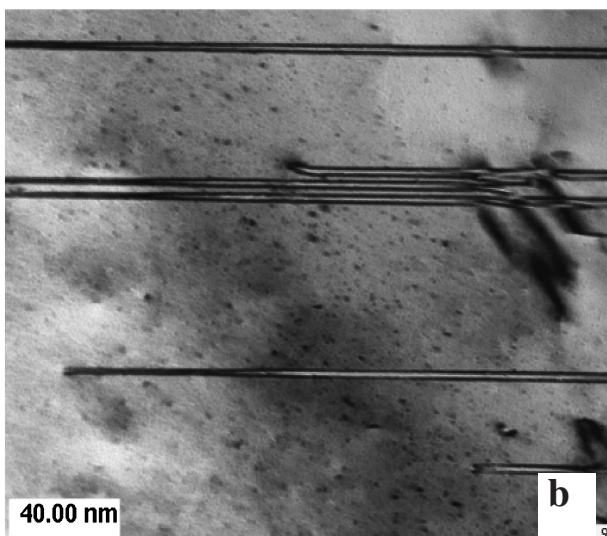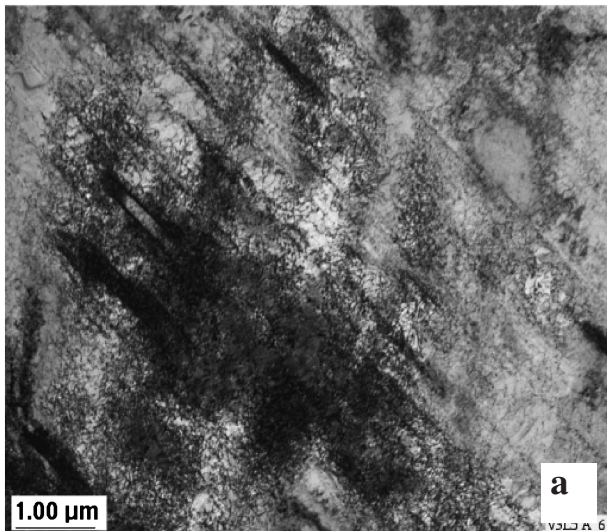
Fig. 12 Highly-deformed microstructures of the $1.1 \times 10^{20} \, n/\text{cm}^2$ material; (a) segregated dislocation band structures, and (b) irradiation-induced "black-spots" and micro-/nanotwins

Fig. 13 Deformed microstructures of the $6.2 \times 10^{20} \, n/\text{cm}^2$ material; (a) inhomogeneouly segregated dislocation band structures, and (b) grain boundary microstructures of wavy contrasts

with increasing strain. Therefore, stress and strain concentrations at grain boundaries as a mechanically induced process is the alternative to the Cr depletion mechanism, causing IG crack initiation above the critical fluence due to the intersection between dislocation channels and/or segregated dislocation bands and grain boundaries. IG cracks would then be initiated at grain boundaries in order to releasing very high stresses accumulated there.

3. Mechanism of TG Crack Initiation

Crack initiation mechanism of TG cracking in the irradiated 304L SS is another concern that should be clarified, because once TG cracking occurs on the surface region of the material it may possibly trigger IG cracking, as noted in the Introduction. A classical concept of TG crack initiation was proposed by Pugh,[19] who insisted that TGSCC occurred by environmentally induced cleavage and propagated by discontinuous brittle fracture (cleavage), though the manner
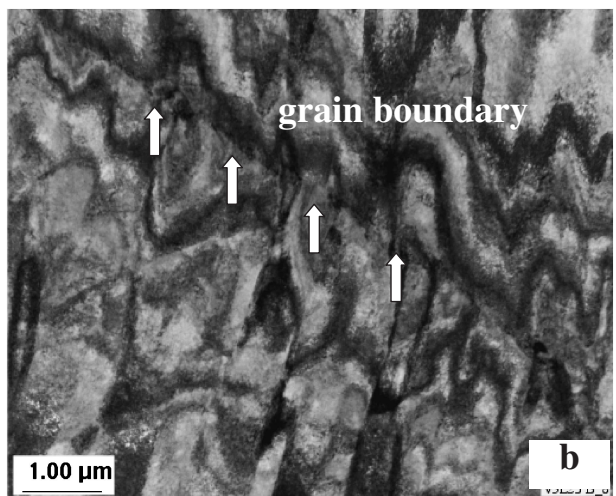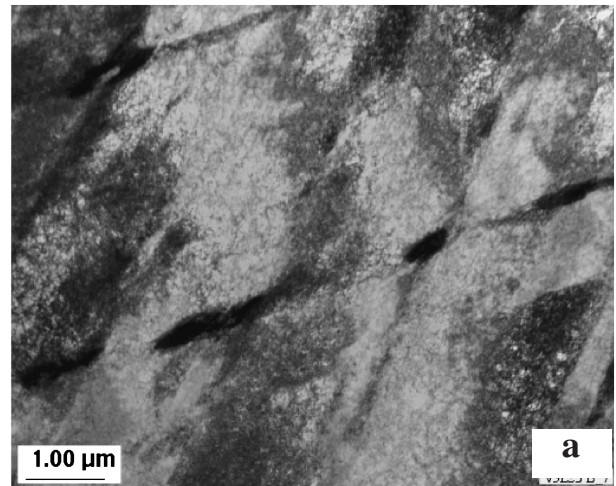
in which the environment induces cleavage in normally ductile alloys has not been determined. This may be true when water contains a certain amount of chemical agents like chlorine and ammonia.

In the present work, TG cracking occurred at a fluence below the critical fluence for IG, at the surface region of the irradiated material (Fig. 4(b)). That should be differentiated from the other type of TG cracking that happens in the interior of the material during the SSRT tests, reviewed by Szklarska-Smialowska, et al.[20] They noted that after the initial IG cracks penetrated into the metal deeply enough, a transition from IG to TG crack propagation was often observed. The process was explained in terms of higher strain rate that is more favorable to induce twin deformation than slip deformation at the IG crack front. In the present discussion, we deal with TG cracking on the surface regions of the material below the critical fluence.

It was found from the superimposed stress-strain curves at $7.5 \times 10^{19} \, n/\text{cm}^2$ (Fig. 2(b)) and the results of fractographic examination (Fig. 6) that the TG cracking on the surface

(a) $7.5 \times 10^{19} n/cm^2$

(b) $1.1 \times 10^{20} n/cm^2$

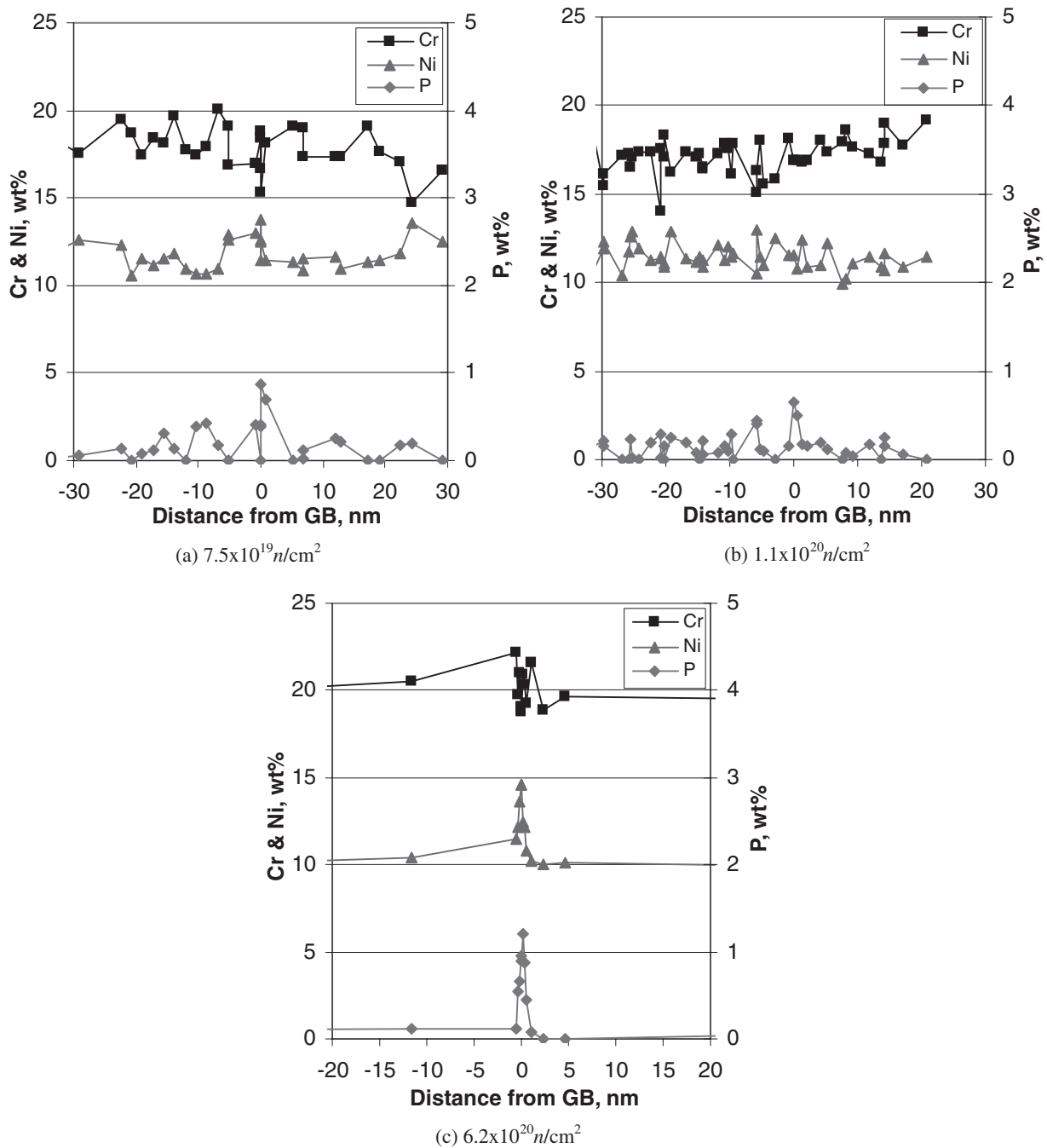(c) $6.2 \times 10^{20} n/cm^2$

Fig. 14 Typical Cr, Ni, and P concentration profiles at grain boundaries of the irradiated samples by FEGSTEM analyses

of the irradiated material initiated and grew in the non-uniform strain region during the SSRT test. The fractographic appearance of the TG cracking resembles that for pseudo-cleavage fracture in fcc metal. Obviously the fracture in a cleavage manner under water environment was brought about by irradiation hardening of the material, since the yield stress at $7.5 \times 10^{19} n/cm^2$ was 1.5 times higher than at the unirradiated condition (Fig. 3(a)). The higher yield strength of the radiation-hardened material is more favorable to deformation twinning, particularly in the non-uniformly deformed region closer to the fracture surface where the CRSS would be allowed to rise even higher with the reduction in

cross-section, as well as within constrained areas such as the annealing twin band that was shown in Fig. 10(b).

A significant difference in the deformed microstructures between the unirradiated and irradiated materials is the presence of numerous deformation-induced microtwins that reside extensively in the areas of a high density of dislocations. Such a high population of deformation twins results in a high frequency of intersections, further constraining dislocation movement, and promoting micro-crack nucleation and initiation. It is likely that the occurrence of a large population of deformation twins is related to the initiation of TG cracking. Therefore we can hypothesize that such a high density of de-
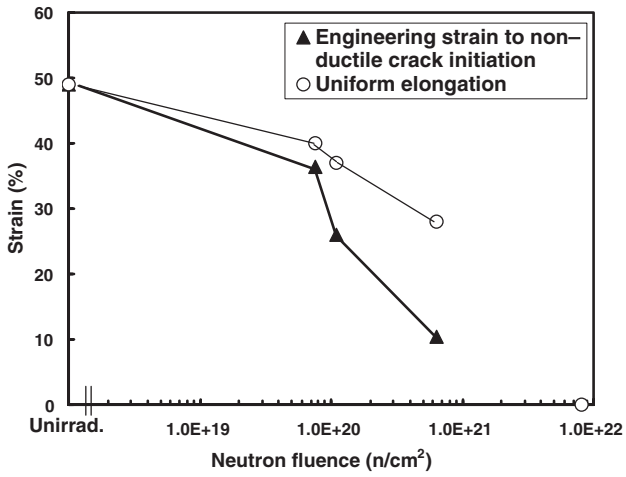
Fig. 15 Engineering strain to non-ductile crack initiation in water as a function of fluence, comparing with uniform elongation
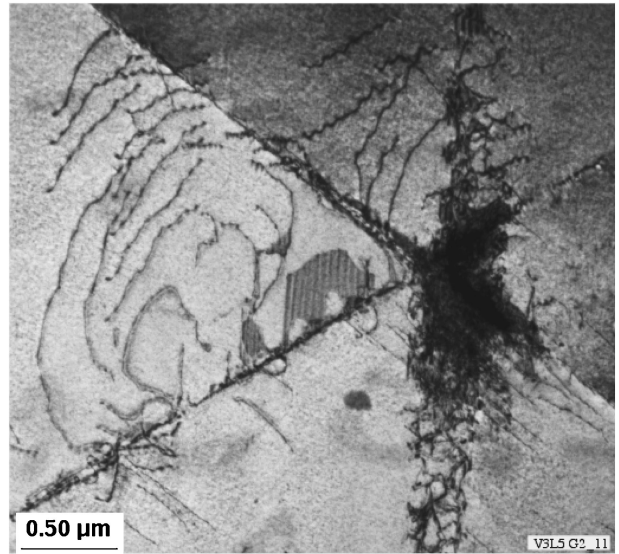

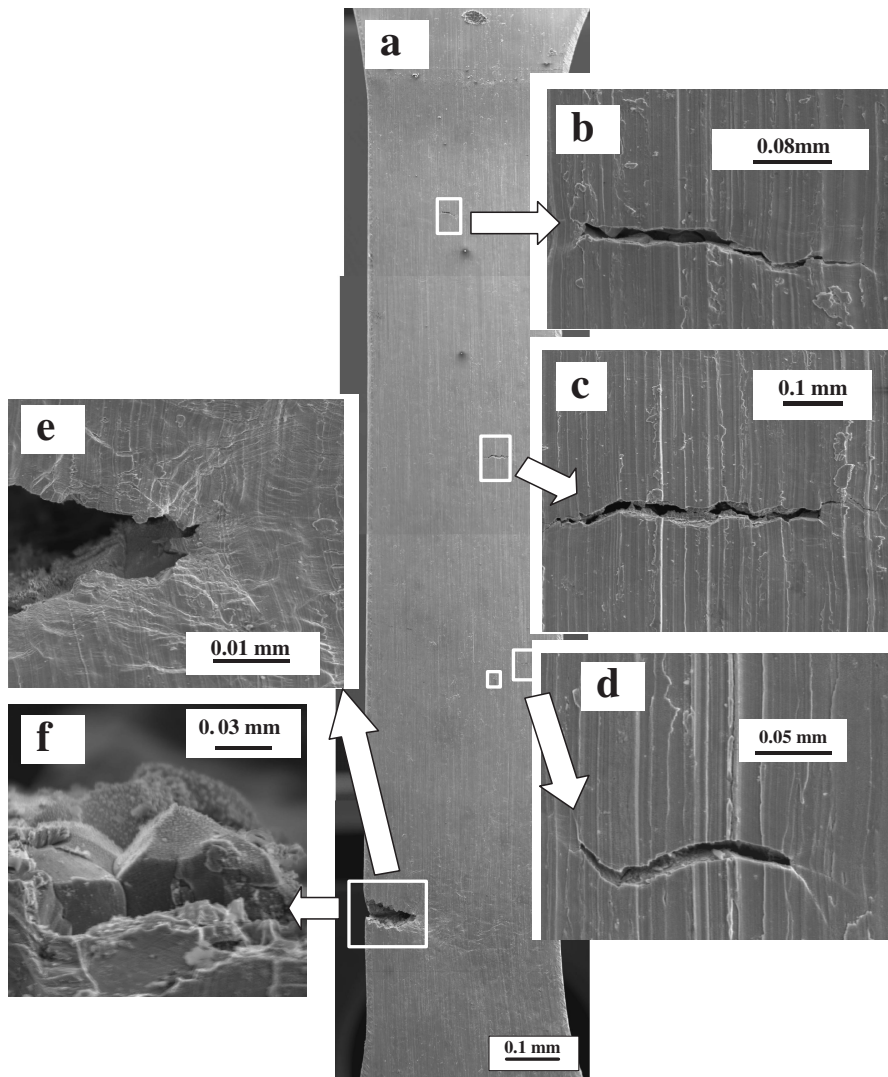Fig. 17 Intersection of dislocation channels in a grain in the early stage of slip deformation at $1.1\times10^{20}\ n/\text{cm}^2$

Fig. 16 Surface appearances of cracks on the $6.2\times10^{20}\ n/\text{cm}^2$ specimen at a plastic strain of about 9% in an interrupted SSRT test in water

formation twins are related to TG cracking in the irradiated material.

In most metallic materials slip generally occurs first and then twins are nucleated when the stress concentrations at dislocation pile-ups exceed the CRSS for twinning.[21] Evidence from fractographic examination show very high stress and strain concentrations happened by an externally applied force in the vicinity of the fracture face, as seen in Fig. 6(b). The relationship between deformation twins, local stress and strain concentrations at twin boundaries and TG crack initiation has been discussed with theoretical calculations and on the bases of experimental observations, suggesting that twin boundaries will become TG crack initiation sites and propagation paths when deformation twins can act as the source of high stress concentration,[22,23] in particular at the intersection of twin deformation bands. Very high stress and strain concentrations will occur at both twin boundaries and grain boundaries into which localized plastic deformation bands terminate. This means that whether or not non-ductile cracks initiate in water is strongly dependent upon the particular stress and strain concentrations at grain boundaries and twin boundaries. Intergranular cracks in the radiation-hardened material can initiate at grain boundaries loaded by the localized plastic deformation bands, while TG cracks can initiate when externally-applied stresses and strains are concentrated at the deformation twin boundaries in the surface regions of strain-hardened grain matrixes. Further work is still required to adequately prove the role of deformation twinning on TG crack initiation though.

V. Conclusion

(1) Intergranular cracking occurred in water above a critical neutron fluence of around $1 \times 10^{20}\,n/cm^2$ which was determined from the results of SSRT test and SEM fractography. The critical fluence is mechanistically supported by the observation of dislocation channeling in the irradiated, deformed microstructure at that fluence, in the absence of Cr depletion at the grain boundaries.

(2) Above the critical fluence, IG cracking initiated in the early stage of inhomogeneous slip deformation. The initiation of IG cracking came earlier with increasing fluence due to earlier onsets of dislocation channeling, and the distribution of IG cracking became wider over the entire surface region of the material with increasing strain.

(3) Below the critical fluence, TG cracking occurred in water on the non-uniformly-strained surface region and in the later stage of plastic deformation of the irradiated material. It is hypothesized that the initiation of TG cracking is related to a high density of deformation twins in the grain matrixes of the irradiated material.

(4) Intergranular cracking in water initiated at grain boundaries inhomogeneously loaded by localized deformation, while TG cracking is inferred to have initiated at the deformation twin boundaries in the irradiated, strain-hardened material. The stress and strain concentrations at grain/ twin boundaries would be the common cause for the non-ductile crack initiation.

References

1) T. M. Angeliu, "Microstructural characterization of L-grade stain less steels relative to the IGSCC behavior in BWR environments," *Proc. 10th Int. Conf. on Environmental Degradation of Materials in Nuclear Power Systems—Water Reactors*, NACE, in CD, (2001).

2) J. N. Kass, W. L. Walker, A. J. Giannuzzi, "Stress corrosion cracking of welde type 304 and 304L stainless steel under cyclic loading," *Corrosion*, **36**, 299 (1980).

3) J. N. Kass, J. C. Lemaire, R. B. Davis, et al., "Comparative stress corrosion cracking behavior of welded austenitic stainless steel pipe in high temperature high purity oxygenated water," *Corrosion*, **36**, 686 (1980).

4) T. M. Angeliu, P. L. Andresen, M. L. Pollick, et al., "The IGSCC behavior of L-grade stainless steels in 288°C Water," *Proc. 8th Int. Symp. on Environmental Degradation of Materials in Nuclear Power Systems—Water Reactors*, ANS, p. 649 (1997).

5) U. Ehrnsten, P. Aaltonen, P. Nenonen, et al., "Intergranular cracking of AISI316NG stainless steel in BWR environment," *Proc. 10th Int. Conf. on Environmental Degradation of Materials in Nuclear Power Systems–Water Reactors*, NACE, in CD, (2001).

6) T. Shoji, "Progress in the mechanistic understanding of BWR SCC and its implication to the prediction of SCC growth behavior in plants," *Proc. 11th Int. Conf. on Environmental Degradation of Materials in Nuclear Power Systems—Water Reactors*, Stevenson, Washington, Aug. 10–14, 2003, p. 588 (in CD), (2003).

7) K. Fukuya, S. Shima, K. Nakata, et al., "Mechanical properties and IASCC susceptibility in irradiated stainless steels," *Proc. 6th Int. Conf. on Environmental Degradation of Materials in Nuclear Power Systems—Water Reactors*, TMS, p. 565 (1993).

8) Ann-Tinn Shen, Chung Shing Chang, "IASCC behavior of 304L stainless steel," *Proc. 11th Int. Conf. Environmental Degradation of Materials in Nuclear Power Systems*, Stevenson, WA, USA, Aug. 10–14, 2003, p. 986 (in CD), (2003).

9) G. S. Was, J. T. Busby, "Role of irradiated microstructure and microchemistry in irradiated-assisted stress corrosion cracking," *Philos. Mag.*, **85**, 443 (2005).

10) S. M. Bruemmer, E. P. Simonen, P. M. Scott, et al., "Radiation-induced material changes and susceptibility to intergranular failure of light-water-reactor core internals," *J. Nucl. Mater.*, **274**, 299 (1999).

11) T. Onchi, K. Dohi, N. Soneda, et al., "Mechanism of irradiation assisted stress corrosion crack initiation in thermally sensitized 304 stainless steel," *J. Nucl. Mater.*, **340**, 219 (2005).

12) T. Onchi, K. Dohi, N. Soneda, et al., "Fractographic and microstructural characterization of irradiated 304 stainless steel intergranularly fractured in inert gas," *J. Nucl. Mater.*, **320**, 194 (2003).

13) J. T. Busby, G. S. Was, E. A. Kenik, "Isolating the effect of radiation-induced segregation in irradiation-assisted stress cor-

rosion cracking of austenitic stainless steels," *J. Nucl. Mater.*, **320**, 20 (2002).

14) K. Fukuya, M. Nakano, K. Fujii, *et al.*, "Role of radiation-induced grain boundary segregation in irradiated assisted stress corrosion cracking," *J. Nucl. Sci. Technol.*, **41**[5], 594 (2004).

15) M. S. Wechsler, "Dislocation channeling in irradiated and quenched metals," *The Inhomogeneity of Plastic Deformation*, ASM, Ohio, 19 (1973).

16) M. Victoria, N. Baluc, C. Bailat, *et al.*, "The microstructure and associated tensile properties of irradiated fcc and bcc metals," *J. Nucl. Mater.*, **276**, 114 (2000).

17) J. I. Cole, J. L. Brimhall, J. S. Vetrano, *et al.*, "Deformation temperature, strain rate, irradiation microstructure effects on localized plasticity in 304L SS," *Proc. 7th Int. Symp. on Environmental Degradation of Materials in Nuclear Power Systems—Water Reactors*, NACE, p. 817 (1995).

18) R. D. Carter, M. Atzmon, G. S. Was, "Deformation and crack-

ing of irradiated austenitic stainless steels," *Proc. 7th Int. Symp. on Environmental Degradation of Materials in Nuclear Power Systems—Water Reactors*, NACE, p. 807 (1995).

19) E. N. Pugh, "Progress toward understanding the stress corrosion problem," *Corrosion*, **41**, 517 (1985).

20) S. Szklarska-smialowska, G. Cragnolino, "Stress corrosion cracking of sensitized type 304 stainless steel in oxygenated pure water at elevated temperatures (Review)," *Corrosion*, **36**, 653 (1980).

21) R. E. Smallman, *Modern Physical Metallurgy*, 3rd Ed., Butterworths, London, 276 (1970).

22) K. S. Sree Harsha, "Stress concentration of terminating twins," *Metall. Trans.*, **12A**, 365 (1981).

23) L. Lemy, "The interaction between slip and twinning systems and the influence of twining on the mechanical behavior of fcc metals and alloys," *Metall. Trans.*, **A12**, 387 (1981).